## Title
Laboratory experiments on the breakup of liquid metal diapirs



## Authors
Wacheul, Jean-Baptiste
Le Bars, Michael
Monteux, Julien
et al.

## Publication Date
2014-10-01

## DOI
10.1016/j.epsl.2014.06.044

Peer reviewed

Earth and Planetary Science Letters 403 (2014) 236–245

Contents lists available at ScienceDirect

Earth and Planetary Science Letters

www.elsevier.com/locate/epsl

# Laboratory experiments on the breakup of liquid metal diapirs

Jean-Baptiste Wacheul [a,b], Michael Le Bars [a,c,*], Julien Monteux [d], Jonathan M. Aurnou [a]

[a] Department of Earth, Planetary and Space Sciences, University of California, Los Angeles, CA 90095-1567, USA
[b] Ecole Normale Supérieure, Paris, France
[c] CNRS, Aix-Marseille Université, École Centrale Marseille, IRPHE UMR 7342, Marseille, France
[d] Laboratoire de Planétologie et de Géodynamique, LPG Nantes, CNRS UMR 6112, Université de Nantes, France

ARTICLE INFO

*Article history:*
Received 21 January 2014
Received in revised form 14 May 2014
Accepted 26 June 2014
Available online 24 July 2014
Editor: C. Sotin

*Keywords:*
metal diapir
breakup
core formation
magma ocean
metal–silicate equilibration
laboratory experiments

ABSTRACT

The validity of the iron rain scenario, i.e. the widely accepted model for the dynamics of iron sedimentation through a magma ocean during the latest stage of the Earth's accretion, is explored via a suite of laboratory experiments. Liquid gallium and mixtures of water and glycerol are used as analogs of the iron and the molten silicate respectively. This allows us to investigate the effects of the viscosity ratio between iron and silicate and to reproduce the relevant effects of surface tension on the fragmentation dynamics. While the classical iron rain scenario considers a population of purely spherical drops with a single characteristic radius that fall towards the bottom of the magma ocean at a unique velocity without any further change, our experiments exhibit a variety of stable shapes for liquid metal drops, a large distribution of sizes and velocities, and an intense internal dynamics within the cloud with the superimposition of further fragmentations and merging events. Our results demonstrate that rich and complex dynamics occur in models of molten metal diapir physics. Further, we hypothesize that the inclusion of such flows into state of the art thermochemical equilibration models will generate a similarly broad array of complex, and likely novel, behaviors.



## 1. Introduction

Differentiation of Earth into a core and a mantle was likely completed within the first tens million years after its accretion (e.g. Stevenson, 1990; Boyet et al., 2003; Boyet and Carlson, 2005). Numerical simulations (Neumann et al., 2012) and geochemical data on meteorites (Yoshino et al., 2003) also show that small planetesimals could have differentiated even earlier when accounting for heating by decay of short-lived radionuclides. There is also strong evidence that the Earth's late accretion is due to collisions with large planetesimals (a tenth to a third of Earth mass), when both the impactor and the proto-Earth were already differentiated (Morbidelli et al., 2012). During accretion, the Earth and other planets in formation underwent several mechanisms of heating: 1) the decay of relatively abundant radioactive elements with short half-life (Merk et al., 2002; Walter and Tronnes, 2004), 2) the conversion of gravitational potential energy by viscous forces during differentiation (Rubie et al., 2007; Monteux et al., 2009; Samuel, 2012), 3) the collisions themselves with the conversion of huge amount of kinetic energy (Safronov, 1978; Kaula, 1979; Reese and Solomatov, 2006; Monteux et al., 2007), these impacts alone being able to generate a local melting resulting in a shallow magma ocean (Tonks and Melosh, 1992). In addition, the primitive atmosphere was certainly much more opaque to IR radiation, so the effect of thermal blanketing was highly efficient (Abe and Matsui, 1985). Thus, according to the simulations, Earth has probably had one or several episodes of global magma ocean, with depths possibly reaching thousands of kilometers (Tonks and Melosh, 1993). In this context, further impacts of differentiated planetesimals would require, in order for the cores of the Earth and the meteorites to merge, that the latter flows through the magma ocean (Fig. 1). This process can be seen as a secondary step of mixing between core and mantle, since it could lead to partial or complete thermo-chemical equilibration between the sinking metal and the molten surrounding silicates, depending on the characteristics of the flow of the core material through the mantle.

The importance of this exchange is an issue for the interpretation of numerous geochemical proxies, such as the tungsten 182 signal. Hafnium ($^{182}$Hf) disintegrates in tungsten ($^{182}$W) with a relatively short half-life of 9 My, comparable with the time scale of core differentiation. They are both refractory but tungsten is siderophile whereas hafnium is lithophile. This is why the

* Corresponding author at: CNRS, Aix-Marseille Université, École Centrale Marseille, IRPHE UMR 7342, Marseille, France. Tel.: +33 4 13552020; fax: +33 4 13552001.
*E-mail address:* lebars@irphe.univ-mrs.fr (M. Le Bars).

http://dx.doi.org/10.1016/j.epsl.2014.06.044
0012-821X/

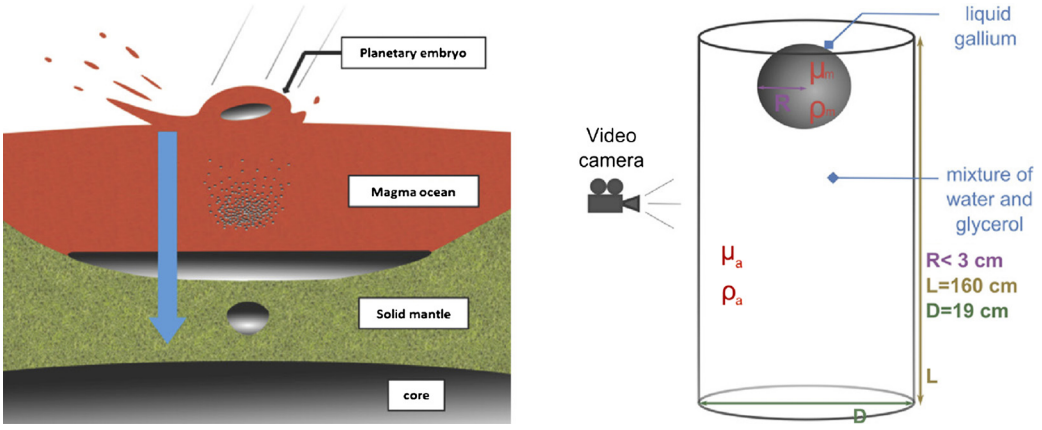


**Fig. 1.** Left: schematic of the metal/silicate separation after the impact of a differentiated planetesimal with the early Earth in reference to the work of Stevenson (1990). The equilibration by diffusion between the impactor's core and the magma ocean during the metal rainfall and later when sinking through the solid mantle as a large diapir is poorly constrained, and strongly depends on the fluid dynamics of the iron sedimentation. Right: schematic of our experiment.

$^{182}$Hf–$^{182}$W system has been used in multiple studies to approximate the age of terrestrial bodies' core (Lee and Halliday, 1996; Harper and Jacobsen, 1996; Kleine et al., 2004). However due to the late impacts and possible mixing that could occur, there are very poor constraints on which event – late impacts or core differentiation – is relevant for the interpretation of the ratio $^{182}$W/$^{184}$W. Then the age given by this proxy could be any intermediary between the initial differentiation of the proto-Earth and the most recent giant impact that it endured, depending on how much $^{182}$W has been absorbed by the asteroid's core during its passing through the mantle (Kleine et al., 2004). The same kind of interrogation can be held against interpretations of the U/Pb proxy, and for the coefficients of partition between metal and silicate, which strongly depend on the details of the small-scale processes at the iron–silicate interface during sedimentation. Actually, these interfacial dynamics influence every mechanism of equilibration by diffusion, such as diffusion of heat and diffusion of momentum by viscosity, both leading to indetermination on the initial thermal state of the mantle and the core, and on the repartition of the energy between these two (Monteux et al., 2009; Samuel et al., 2010). Thus, in order to model the evolution of both Earth's core and mantle, it is important to understand the fluid dynamics at the drop scale during the iron sedimentation (Solomatov, 2000). Towards this goal, we present here novel laboratory experiments investigating the fluid dynamics of sedimenting liquid metal droplets.

## 2. Parameters controlling the fluid dynamics of the iron sedimentation

The equilibration between the iron and molten silicate strongly depends on the typical size of the metal entities. Indeed, for a given volume of metal, a single large diapir would fall rapidly through the magma ocean with a relatively small surface of exchanges, while the fragmentation of the same volume of iron through a large number of small structures broadens the surface area of exchanges and slows down the falling velocity, hence extending the time during which iron and silicate equilibrate. Note that in the present paper, we generically use the term diapir to designate any large blob of fluid moving through an ambient fluid via the action of buoyancy forces.

Several approaches have been developed in order to give a physically coherent description of what happens when a liquid iron diapir falls through a magma ocean, and ultimately to provide a time scale for the equilibration. At first order, the shape of the falling diapir is dominated by two forces. The surface tension tends to stabilize a spherical shape, while the dynamic pressure deforms the diapir and tears it apart. Let us assume for instance, a typical diapir with a radius $R_0 = 10$ km falling at the inviscid, free fall Newtonian velocity $V$ valid for a rigid sphere

$$V \simeq \sqrt{\frac{\Delta\rho}{\rho_a} g R_0}, \tag{1}$$

where $\rho_a$ is the silicate density ("$a$" standing for "ambient"), $\Delta\rho$ is the density difference between iron and silicate, and $g$ is the gravitational acceleration. Assuming an Earth with more than half its final mass, $V$ is close to 1 km/s. The Re number for the flow in the mantle, which estimates the ratio of the inertial and viscous forces, is

$$Re_a = \frac{\rho_a V R_0}{\mu_a} \gtrsim 10^{10}, \tag{2}$$

where $\mu_a$ is the silicate dynamic viscosity. This large $Re$ value provides an *a posteriori* validation of the inviscid velocity estimate provided by Eq. (1). It also implies that dynamic pressure scales as the inertia. On the other hand, the characteristic strength of surface tension is directly linked to the radius of curvature of the surface, so its order of magnitude roughly depends on the radius of the spheroid diapir $R_0$. A good estimation of the stability of a diapir is given by the Weber number, which is the ratio of the inertial and surface tension forces:

$$We_a = \frac{\rho_a V^2 R_0}{\sigma}, \tag{3}$$

where $\sigma$ is the coefficient of surface tension. For $We \gg 1$, diapirs are unstable and break-up. Below some threshold of order 1 (e.g. $We_c = 6$ for rain drops, see Villermaux and Bossa, 2009), surface tension and inertia compensate, and the diapir is stable. This widely used breakup criterium (e.g. Tonks and Melosh, 1992; Rubie et al., 2003; Dahl and Stevenson, 2010; Deguen et al., 2011) allows a calculation of the maximal radius for stable diapirs, given some hypothesis regarding its falling speed. For the simple Newtonian velocity scaling given by (1), the maximal radius corresponds to

$$R_{cap} \simeq \sqrt{We_c \frac{\sigma}{\Delta\rho g}}, \tag{4}$$

which is about 1 to 2 cm for the Earth's iron–silicate system. Such a criterium is well known in the case of water drops in the air, for which it has been confirmed by experiments (Villermaux and Bossa, 2009). It has also been supported by a recent numerical study designed for the case of an iron diapir in molten

silicate (Samuel, 2012). In this study, the initial spherical diapir flattens, then breaks up within a distance of no more than 10 diapir radii. The diapir's sons keep breaking up, cascading downward to the scale $R_{cap}$ where surface tension compensates the pressure forces. However, in these axisymmetric simulations, the breakup is not actually computed, but is supposed to occur shortly after the topological change from pancake to torus. Thus, the size of the resulting drops remains unknown. According to this scenario, there is no way for a 10 km radius diapir corresponding to a Weber number above $10^{14}$ to remain entirely intact during its fall. It should rapidly break up into a cloud of drops of radius $R_{cap}$, *i.e.* the so-called "iron rain". Then, most models of metal–silicate equilibration (e.g. Rubie et al., 2003; Ulvrová et al., 2011; Samuel, 2012) assume that all iron drops have an identical and fixed spherical shape with a radius equal to $R_{cap}$ and a unique sedimentation velocity based on free fall models.

On the other hand, for diapirs with a radius of 10 km and above, the Weber number is so large (above $10^{14}$) that its dynamics are controlled by the inertia of the flow only, allowing one to completely ignore the effects of surface tension. The resulting miscible models lead to interesting findings. For instance, Deguen et al. (2011) supposed that the diapir rapidly becomes a cloud of drops that then evolves in a coherent manner as a buoyant thermal, whose radius grows linearly with depth because of turbulent mixing with the outside. They found that for a shallow magma pond created by an impact as for a deep magma ocean (Deguen et al., 2014), there should be enough dilution between metal and silicate for them to reach chemical equilibration. On the contrary, Dahl and Stevenson (2010) considered a diapir with an almost constant shape eroded by Raleigh–Taylor and Kelvin Helmholtz instabilities. Their conclusions were very different: erosion was found to be insufficient to allow for full equilibration for diapirs with a radius above 10 km.

Open questions thus remain on all stages of the iron sedimentation, from the large-scale dynamics to the behavior at the smallest scales, where surface tension modifies the modalities of diffusive exchanges. In this context, the numerical study by Ichikawa et al. (2010), in agreement with the results for water drops in the air (Villermaux and Bossa, 2009), pointed out that the cloud of drops contains a whole distribution of sizes and not just a single one (Karato and Murthy, 1997). Furthermore, the distribution of speeds and the relation between size and speed of drops are not trivial, supporting the idea that the iron rain scenario with a single size and speed may be inaccurate. However, the conclusions of Ichikawa et al. (2010) are supported mostly by 2D numerical simulations, where surface tension is not properly rendered. Hence they still need confirmation.

In addition, it is worth noting that all previous studies of the stability of diapirs have neglected the influence of the viscosity ratio between the ambient fluid and the metal

$$r_\mu = \frac{\mu_a}{\mu_m}. \tag{5}$$

When the magma ocean cools down, or as the diapir goes deeper into the mantle, the magma becomes closer to the solidus and contains more crystals. Therefore, the viscosity of the magma is expected to increase from $10^{-3}$ to $10^{2}$ Pa s, corresponding to $r_\mu$ ranging from 1 to $10^5$ (Deguen et al., 2011; Samuel, 2012). Such a large viscosity ratio is known to have a significant effect on the shape of falling drops (e.g. Bonometti and Magnaudet, 2006; Ohta et al., 2010). Indeed, from the continuity of the velocity and the stress tensor at the drop interface, a large $r_\mu$ in a large Reynolds number flow implies intense internal recirculations inside the drop, which then deforms and may be dynamically stabilized. This has not been investigated in a geophysical context.

**Table 1**
List of relevant parameters and typical Earth's and experimental values.

| Symbol | Parameter | Value for the Earth | Value in our experiment |
|---|---|---|---|
| $\rho_a$ | ambient fluid density | 3000 kg m$^{-3}$ | 997–1260 kg m$^{-3}$ |
| $\rho_m$ | liquid metal density | 7000 kg m$^{-3}$ | 6095 kg m$^{-3}$ |
| $\mu_a$ | ambient fluid viscosity | $10^{-3}$–$10^{2}$ Pa s | $10^{-3}$–1 Pa s |
| $\mu_m$ | liquid metal viscosity | $10^{-3}$ Pa s | $1.9 \times 10^{-3}$ Pa s |
| $r_\mu$ | viscosity ratio | 1 to $10^5$ | 0.5 to 500 |
| $\sigma$ | surface tension | 1 J m$^{-2}$ | 0.7 J m$^{-2}$ |

Here we report the first experiments designed to simulate the last stages of the fragmentation process with realistic values of the iron–silicate viscosity ratio and relevant behaviors regarding the effects of surface tension on the fragmentation dynamics. The set-up is presented in Section 3. In Section 4, we investigate the variety of stable shapes for iron drops, as well as their mutual interactions and dynamics after the initial breakup. The measured distributions of size and velocity are presented in Sections 5 and 6, highlighting the influence of the viscosity ratio. The relevance of the complex fluid dynamics shown by our experiments to the Earth is illustrated in Section 7 by a simple equilibration model based on our results. Conclusions and open questions are given in Section 8.

## 3. Set-up and methods

Our experimental set-up is sketched in Fig. 1. As an analogue for the magma ocean, we use a 160 cm high cylindrical tank, with a diameter of 19 cm, filled with a mixture of water and glycerol. The glycerol (resp. water) has a dynamic viscosity of 1.08 Pa s (resp. 0.00093 Pa s) at room temperature (23 °C): the mixture of the two allows us to explore a range of 3 orders of magnitude for the viscosity of the ambient fluid $\mu_a$, with a density ranging from $\rho_a = 1260$ kg m$^{-3}$ for pure glycerol to $\rho_a = 997$ kg m$^{-3}$ for pure water. As an analogue for the liquid iron diapir, we use liquid gallium. It has a viscosity $\mu_m = 1.9 \times 10^{-3}$ Pa s and a density $\rho_m = 6095$ kg m$^{-3}$ (King and Aurnou, 2013). The gallium is initially contained in a latex balloon at the top of the set-up; the ballon is then popped by a syringe needle at the beginning of the experiment. This method has two advantages: the amount of gallium is precisely known by weighing the balloon, and since the retraction of the balloon occurs within about 1/50 s, the diapir has no initial speed and its initial shape is the one imposed by the balloon. The fall of the diapir is then recorded by a high speed USB camera at 136 frames per second, with a resolution of 196 × 1280 pixels (examples of these videos can be viewed at https://www.youtube.com/watch?v=g-AmGmWWK1o&list=UU7u8FUioww0nKsdXPO6emhA). In addition to this camera, higher resolution videos of the lower part of the experiment are taken at 60 frames per second with a resolution of 1280 × 720 pixels. Beyond direct visualization, the videos are used to recover the shape and velocity of the droplets, after removing the background and after binarization. Each droplet in a selected frame is detected using the Matlab Image Processing toolbox, and an equivalent radius is retrieved by measuring its apparent area $A$ and applying the formula $r = \sqrt{A/\pi}$. This is a lower estimate since the drops are oblate at different degrees. We also construct space–time diagrams by extracting the same horizontal line from all frames of a chosen video. The resulting image then gives us the horizontal radius of each droplet reaching the selected depth as well as its arrival time, hence its mean fall velocity.

Relevant parameters are listed in Table 1 in comparison with Earth's values. Experiments were run with 6 different sizes of the initial diapir ranging from an equivalent radius of 14 mm to 30 mm, and with 4 viscosities of the ambient fluid 0.001, 0.01, 0.1 and 1 Pa s. In the inertial regime, the characteristic velocity of the

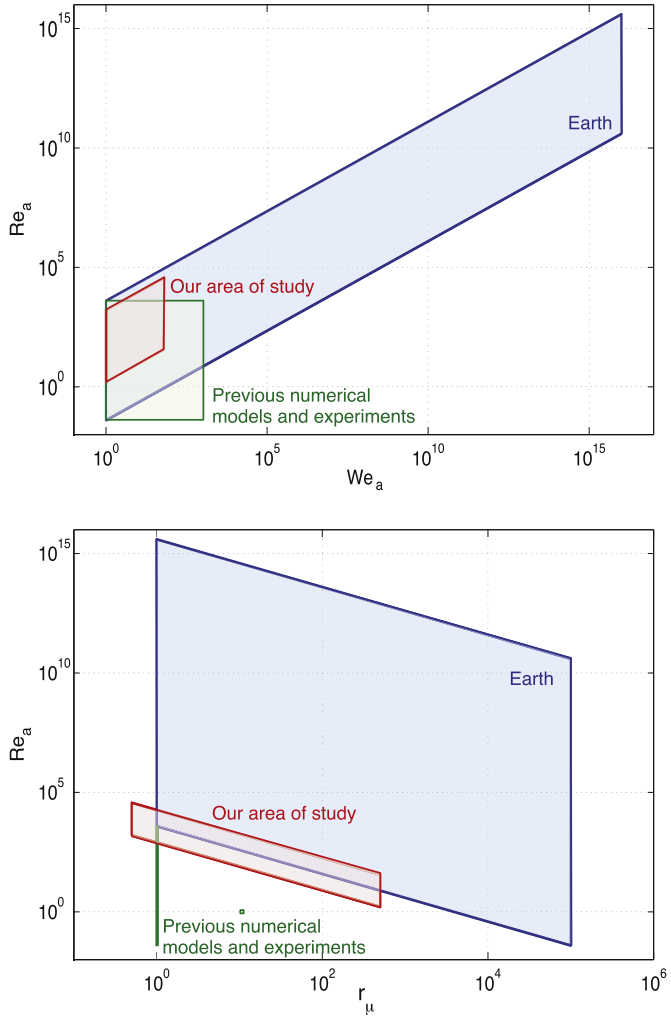


**Fig. 2.** In blue, area of the parameter space associated with the fall of iron diapirs in the context of Earth's accretion. Variations are due to changes in the viscosity of the magma ocean and in the diapir radius, ranging from its initial value to the radius corresponding to a Weber number of 1. For comparison, the area explored by previous studies (Ichikawa et al., 2010; Samuel, 2012; Deguen et al., 2014) is shown in green, whereas the parameter space explored by the present study is shown in red. (For interpretation of the references to color in this figure legend, the reader is referred to the web version of this article.)

flow scales as the Newtonian velocity introduced in Eq. (1). Then, the dynamics is entirely characterized by four dimensionless parameters: the density ratio $\Delta\rho/\rho_a$, the viscosity ratio $r_\mu = \mu_a/\mu_m$, and the Newtonian Reynolds and Weber numbers $Re_a$ and $We_a$ (based on the Newtonian velocity). In our experiment, $\Delta\rho/\rho_a$ remains almost constant at about 5 (the ambient density only marginally varies with the proportion of water), which means that as in the geophysical setting, density changes are of order 1, such that the Boussinesq approximation cannot be applied. With the accessible range of initial diapir radii, we are able to produce initial Reynolds numbers from 10 to $4 \times 10^4$ and initial Newtonian Weber numbers from 14 to 64. As shown in Fig. 2, this is obviously limited compared to the possible geophysical values, especially for diapirs with large initial radius. But even if the dynamic similitude between the experiment and reality is not exact, the experiments are capable of reaching the relevant dynamical regime, with a fully turbulent flow and a Weber number above the critical value for breakup. Furthermore, the similitude is exact for diapir radii around the decimeter scale, hence for the final stages of the fully-developed iron rain. Note finally that our experiment is the first one to take into account the effects of the viscosity ratio, which spans the range 0.5–500 in our set-up.

## 4. Zoology of the breakup

The results of 3 experiments in pure glycerol with different initial radius of the diapir are shown in Figs. 3A, 3B and 4. Fig. 5 shows a closer look of the various possible shapes of gallium drops obtained in the experiment presented in Fig. 4. According to the classical iron rain scenario applied to our experimental set-up, any diapir with a Weber number larger than 6 should rapidly give rise to a cloud of spherical drops with a single characteristic radius $R_{cap} = 1$ cm that should fall with a Newtonian velocity $V = 74\ \mathrm{cm\,s^{-1}}$, without any further dynamical change. This is not the case.

For the lowest initial radius (Fig. 3A), the diapir is stable even if its Weber number is above the known threshold 6 (note that the effective Weber number is $\simeq$9, calculated using the measured falling velocity instead of the scaling given by Eq. (1)). One can also notice that its equilibrium shape is not spherical: the drop takes the form of a cap, where the intense internal recirculation driven by viscous coupling with the ambient fluid stabilizes the non-spherical shape of the molten metal droplet (see also the sketch in Fig. 5B). The viscosity ratio strongly influences the shape and the condition for stability of a single structure, as found in the studies of Bonometti and Magnaudet (2006), Ohta et al. (2010) using axisymmetric numerical simulations. There is a clear tendency for large viscosity ratios to stabilize the drops, and the diapir shown in Fig. 3A is indeed unstable for $r_\mu$ below 50 (not shown here). According to results in Bonometti and Magnaudet (2006), Ohta et al. (2010), which are coherent with our experimental observations, the critical Weber number can actually be more than one order of magnitude larger than the classically used value $We_c = 6$, depending on the viscosity ratio and the initial shape of the drop.

The slightly larger diapir shown in Fig. 3B rapidly breaks up into three large caps plus some smaller drops. A striking point here is that after this initial break-up, the dynamics is not frozen: the three caps interact and two of them finally merge to re-build a larger diapir. For comparison, the same experiment but with an ambient viscosity 100 times less viscous is shown in Fig. 3C. The initial behavior of the diapir is similar but the breakup dynamics is clearly different, even if the Weber number is the same in both experiments. The Reynolds number is greater in Fig. 3C because of the smaller ambient viscosity; but comparing both series of pictures, one can notice that the falling velocities are close in the two experiments: both cases are in the Newtonian regime, and changes in $Re_a$ cannot explain changes in the fragmentation behavior. Thus, we argue that the differences between Figs. 3B and 3C are due to viscosity ratio effects, which allow for the dynamical stabilization of larger drops by strong internal recirculations in case 3B.

The dynamics of initially large diapirs systematically follows the series of stages illustrated in Fig. 4: after a short acceleration, we observe waves forming on the surface of the diapir, qualitatively similar to the description of Dahl and Stevenson (2010). But almost simultaneously, the diapir flattens as the wave amplitudes rise: it evolves towards a thin wavy sheet where the axisymmetry is fully broken. It breaks up shortly after this stage: holes appear in the sheet, the transient ligaments retract and break-up. The drops resulting from this burst have various sizes and shapes, and the biggest ones continue to break up in the same way until a steady-state is reached. The whole process can be seen as a downward cascade toward small scales where surface tension is important. However, we also observe multiple coalescence of droplets several times in a row, corresponding to a non-linear inverse cascading process. From the experimental videos, we see that

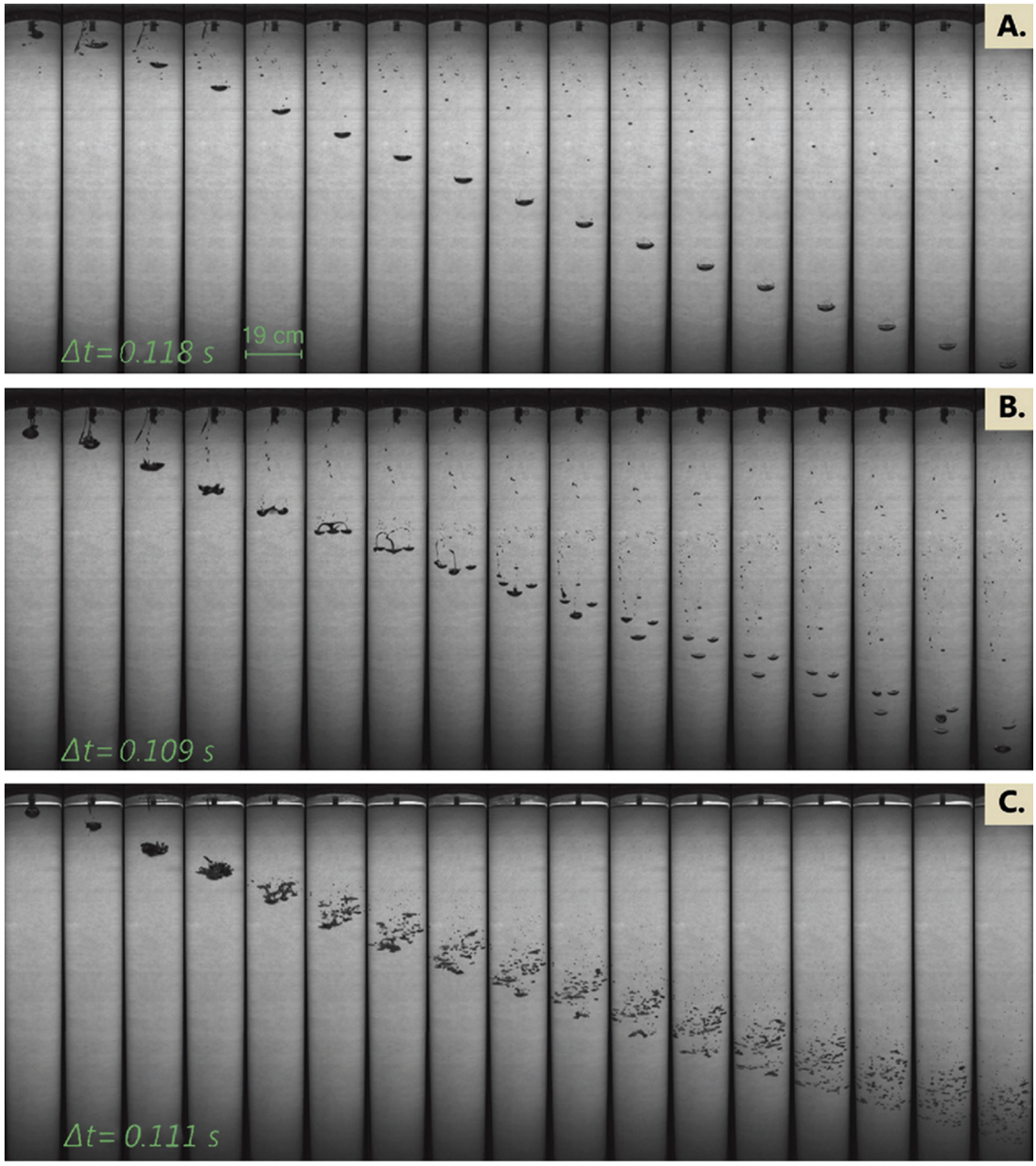


**Fig. 3.** Successive snapshots with a fixed time interval for 3 experiments. A: Fall of a 14 mm initial radius diapir in pure glycerine, corresponding to $Re_a = 12$, $We_a = 14$ and a viscosity ratio of 500. The diapir has a stable cap shape. B: same as A but for a 23 mm initial radius diapir, corresponding to $Re_a = 24$ and $We_a = 37$. The diapir breaks up in 3 main cap-shaped stable drops of close sizes. C: same as B but for an ambient fluid 100 times less viscous, corresponding to $Re_a = 2400$, $We_a = 37$ and a viscosity ratio of 5.

small drops accelerate and merge when they are near bigger drops whose rear recirculation engulfs them. One can argue that the narrowness of our experiment limits the spreading of the metallic droplet cloud, thereby enhancing the typical frequency of droplet collisions. But as noted above, coalescence happens even if there are very few drops. We thus believe that this inverse cascade process is also relevant in larger domains, as for instance in magma oceans.

Fig. 5A shows a closer instantaneous view of the droplet cloud once the steady-state is reached. A whole distribution of shapes and sizes is observed. Large drops have a cap shape stabilized by internal recirculation (see Fig. 5B), and the smallest drops adopt a spherical shape; a continuity of flattened ellipsoidal shapes is observed in between.

We have also observed a novel metastable structure (Fig. 5C) formed during the breakup of the biggest diapirs. These structures look like a hot air balloon and fall slowly relative to other droplets of comparable size. From slow motion videos of their formation and disappearance, we have inferred that they are bubbles of gallium enclosing glycerol (see Fig. 5D), similar to bubbles of soapy water in air. This bubble structure explains their relative stability as well as their anomalously low settling velocity for their rather large size.

## 5. Distribution of sizes and influence of the viscosity ratio

Fig. 6 shows the cumulative distribution of droplets sized obtained from the breakup of the largest class of diapir for a viscosity ratio of $r_\mu = 50$. This corresponds to $Re_a = 368$ and $We_a = 64$. Taking into account the resolution of the video (9.0 pixels $\mathrm{cm}^{-1}$), we are able to detect the size of drops larger than 0.6 mm in radius, the smaller ones being detected as drops of 0.6 mm. The

**Fig. 4.** Successive snapshots with a fixed time interval $\Delta t = 0.18$ s for a 30 mm initial radius diapir falling through pure glycerol, corresponding to $Re_a = 37$, $We_a = 64$ and a viscosity ratio of 500. One can notice that the mean speed of the front of the diapir is rather constant.

breakup of metal diapirs does not create droplets of one single size but a whole distribution of equivalent radii, in agreement with the simulations of Ichikawa et al. (2010). Because the formation of drops results from the generic process of ligament rupture, their size distribution is well fitted by a Gamma distribution, whose probability density function $p$ writes:

$$p(x) = \frac{x^{k-1} e^{-x/\theta}}{\theta^k \Gamma(k)}, \tag{6}$$

where $k$ is the shape of the Gamma distribution, $\theta$ its scale, and $\Gamma(k)$ is the Gamma function evaluated at $k$. Such a Gamma distribution of droplet sizes is similar to the one obtained in the case of water drops in the air (Villermaux and Bossa, 2009). Note however that in this last case, the viscosity ratio is reverse (i.e. the more viscous fluid is inside) and the shapes of the obtained drops are very different. Our distribution is tightened around a mean radius of 4 mm. This value can be related to a breakup criterion, now understood in a statistical sense: surface tension sets the characteristic length scale of the distribution, the mean radius. Using our experimental results, the critical Weber number corresponding to this radius is $We_c \simeq 1$. The distributions obtained for diapirs with different initial sizes are similar to the one shown in Fig. 6, and so is the measured mean radius, provided that these diapirs are large enough to create a distribution of sizes that converges statistically. This condition is verified for the 4 biggest classes of diapirs that we have produced.

Fig. 7 shows series of snapshots from 4 experiments with the same initial diapir but different viscosity ratios. With our present set-up, because a large number of drops are superimposed on the video images, it was not possible to detect their individual contours for a viscosity ratio smaller than 50. Hence we could not perform a systematic quantitative study of the sizes distribution as a function of $r_\mu$. But relying on direct observation, we see that there is a clear tendency for large viscosity ratios to stabilize bigger drops, as already noticed in Section 4 for single structures. In all cases, we expect to systematically recover a Gamma-type distribution for the equivalent radii. This means that the distributions always have the same shape, with a peak at a small scale corresponding to $We_c \simeq 1$, and an exponential tail. But we expect the slope of this tail to be significantly more gentle when the viscosity ratio increases. This corresponds to a decreasing value of the shape of the Gamma distribution: for instance, Villermaux and Bossa (2009) found a shape value of 4 for the breakup of water in the air (viscosity ratio $2 \times 10^{-2}$), while we find a shape of 2.2 for a viscosity ratio of 50, as shown in Fig. 6.

## 6. Simultaneous distributions of sizes and velocities

The interactions between the droplets lead to a wide range of sizes and velocities in our experiments. Fig. 8 shows the distribution of sizes and speeds for a viscosity ratio $r_\mu = 50$ and a diapir with an initial radius of 23 mm, using the values obtained from a space–time diagram at a distance of 140 cm from the initial position of the center of mass of the diapir. It is plotted in the same way as in Ichikawa et al. (2010). The fact that velocities are calculated from the travel time through the tank averages out a large part of the variability due to raw turbulence and allows us to then consider the mean structure of the flow. Interestingly, the drops' velocities do not follow a Newtonian scaling based on their individual radius, even when adjusting the pre-factor (see Fig. 8). This result seems to validate the entrainment hypothesis described by Deguen et al. (2011, 2014): after the breakup, the drops fall as an interacting cloud whose velocity is determined by the inertia of the whole flow, related to the initial mass of the diapir. Additional fluctuations are related to the turbulent mixing and interactions between drops.

## 7. Typical equilibration length

We can estimate a rough length scale of equilibration following the same reasoning as in Samuel (2012), but using the distribution

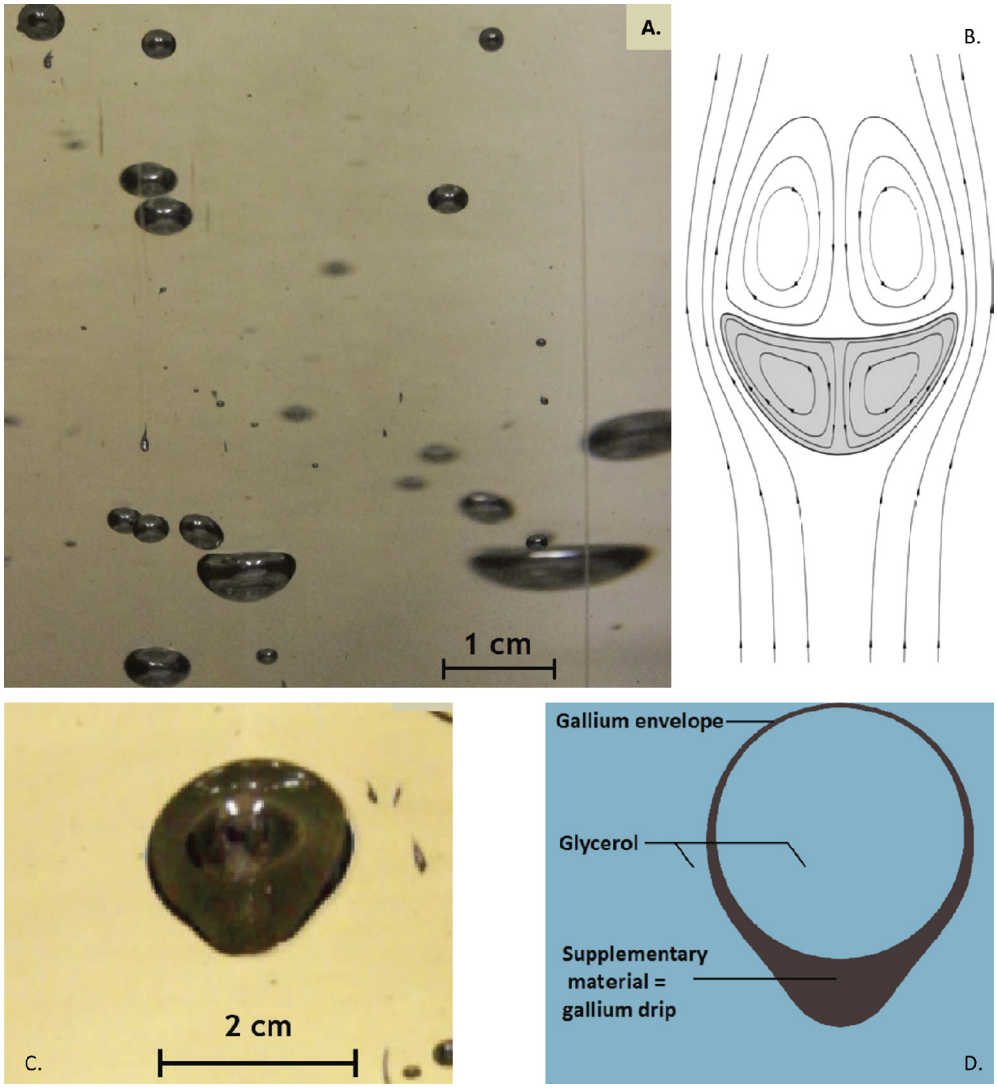


**Fig. 5.** A: drops of liquid gallium of various sizes falling through pure glycerol. Several intermediates between cap shape and spherical shape are present. B: expected streamlines of the relative flow within and around a falling diapir with a cap shape (shown in gray). C: gallium bubble enclosing glycerol formed during the breakup of a 30 mm radius diapir in pure glycerol. Due to its reduced buoyancy compared to full gallium drops, it falls slowly. These structures last from one tenth of a second to several minutes. D: schematic of a gallium bubble.

of sizes and velocities found in our experiments. Note that the relatively simple equilibration models shown below are meant only for illustration of potential consequences of the complex dynamics exhibited in our experiments. The question of geochemical equilibration clearly deserves more detailed studies.

In our model, we neglect the breakup distance and consider that the distribution of sizes and speeds has reached a steady state. From our observations, from simulations (Samuel, 2012) as well as from previous experiments (Deguen et al., 2014), breakup occurs within a typical length scale of a few initial radii, so the previous hypothesis is valid for initial entities at least 10 times smaller than the mantle depth: we choose here an initial diapir of radius 10 km sedimenting in a magma ocean with a minimum depth of 100 km. We suppose that the metal concentration $C_m$ in a chemical element of interest (e.g., Ni, Co, W, Hf) is uniform inside each drop and that it evolves following a simple Fick's law

$$\frac{4\pi}{3} r^3 \frac{dC_m}{dt} = -4\pi r^2 \kappa \frac{C_m - C_{m,eq}}{\delta_{BL}}, \tag{7}$$

where $r$ is the drop radius, $\kappa$ the chemical diffusivity coefficient of typical order $10^{-8}$ m$^2$ s$^{-1}$, and $C_{m,eq}$ the equilibrium concentration. We further assume that the thickness of the chemical boundary layer $\delta_{BL}$ scales as $\delta_{BL} = \sqrt{2\kappa r/v}$, where $v$ is the local speed

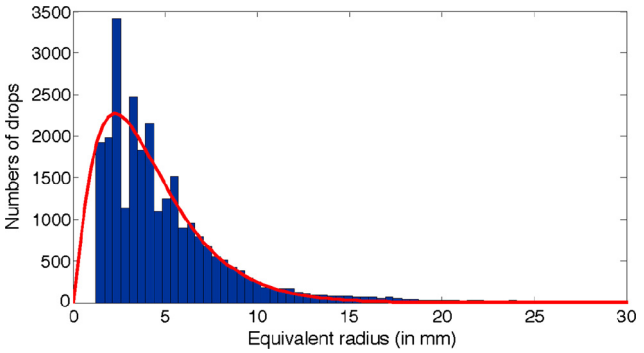


**Fig. 6.** Histogram of the equivalent radius of the droplets created by the breakup of a 30 mm initial radius diapir falling through a mixture of glycerol and water (in blue) and best fitting Gamma distribution (in red, with shape 2.2 and scale 1.9). Dimensionless parameters of the experiment are $Re_a = 368$, $We_a = 64$ and $r_\mu = 50$. The low cutoff radius is set by the resolution of the video to 0.6 mm. A large number of measurements is necessary for obtaining converged statistics. This cumulative distribution was thus constructed from 6 runs of the same experiment and using the last 10 frames of each video, i.e. once a statistically steady state is reached and before the fastest droplet touches the bottom of the tank. (For interpretation of the references to color in this figure legend, the reader is referred to the web version of this article.)

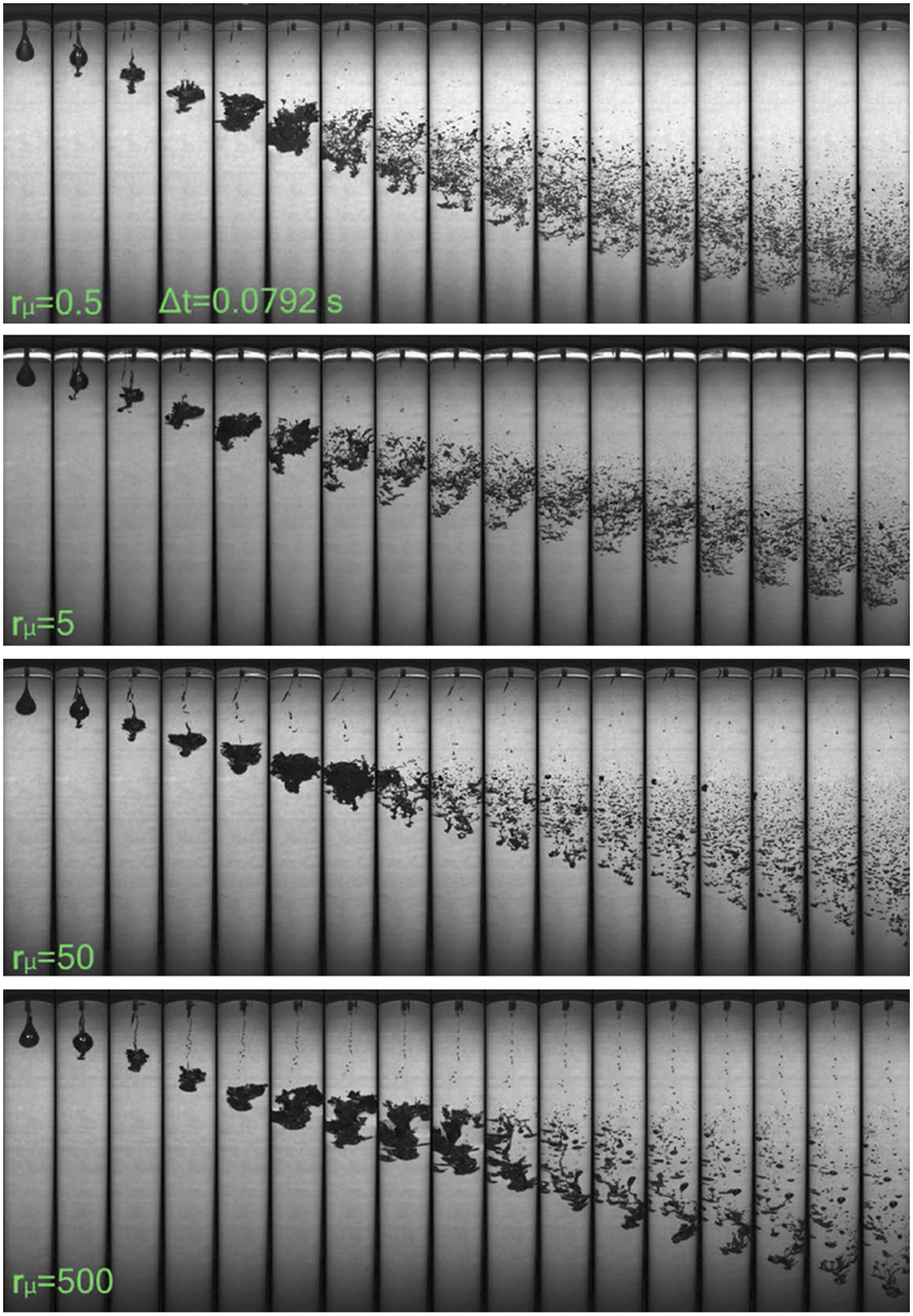


**Fig. 7.** Series of snapshots of the diapirs evolution for 4 runs of the experiment with a 31 mm initial radius diapir. From top to bottom, only the viscosity of the ambient fluid increases; the corresponding viscosity ratios are 0.5, 5, 50, and 500. Rigorously, changing the ambient viscosity also changes the Reynolds number. But it may be noticed from the snapshots that the mean sedimentation velocities in the four cases are comparable, and, hence, largely independent of the ambient fluid viscosity, as expected in the Newtonian limit. We argue then that the various observed dynamics are primarily related to changes in the viscosity ratio.

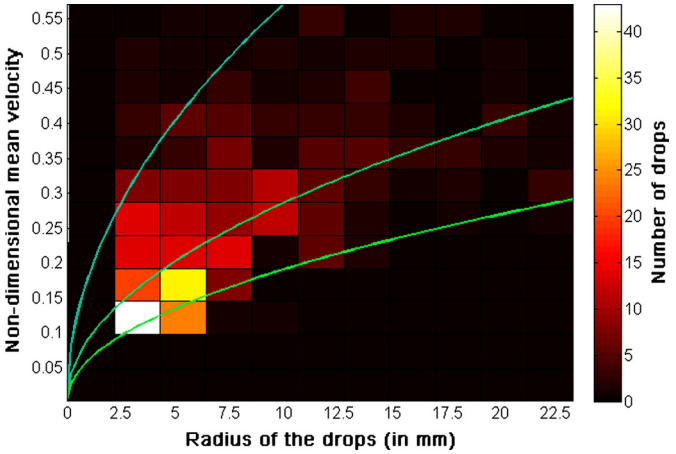


**Fig. 8.** Distribution of the drops equivalent radii (in mm, along the $x$-axis) and speeds (non-dimensionalized by the Newtonian speed of the initial diapir, along the $y$-axis). The initial radius of the diapir is 23 mm and the viscosity ratio is 50, which gives $Re_a = 244$ and $We_a = 37$. Three curves of the corresponding Newtonian velocity scaling (1) with a prefactor respectively equal to 1, 1/2 and 1/3 from top to bottom, are shown in green. (For interpretation of the references to color in this figure legend, the reader is referred to the web version of this article.)

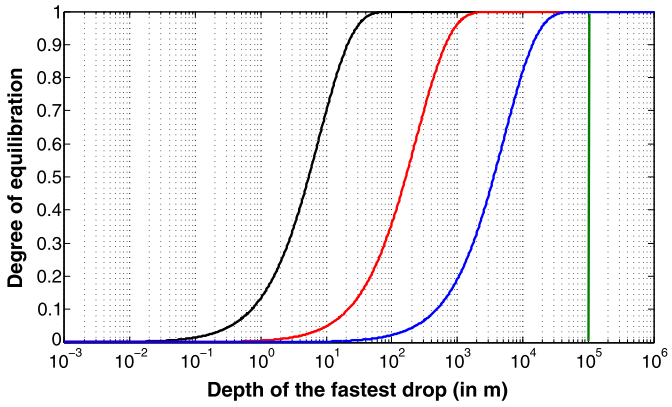


**Fig. 9.** Degree of equilibration of a cloud of droplets resulting from the fragmentation of an initially 10 km radius diapir and falling through a magma ocean. The classical iron rain scenario is shown in black for reference. Two scenarios derived from the statistics of our experiments with an initial radius $R = 30$ mm and $r_\mu = 50$ are also shown, where the global speed of the drop cloud is taken as the Newtonian velocity of the initial 10 km radius diapir. In red, the local speed of the drops is derived from the distributions shown in Fig. 8. In blue, the local speed is given by the Newtonian scaling law for each drop radius. Note that the present model neglects the breakup distance of the initial diapir. For an initial diapir of radius 10 km, this implies a minimum depth of the magma ocean of 100 km, shown by the vertical green line. (For interpretation of the references to color in this figure legend, the reader is referred to the web version of this article.)

of the flow around the droplet, assumed to be constant (following Samuel, 2012). We define the degree of equilibration as

$$C^*(t) = \frac{C_m(t) - C_m(t=0)}{C_{m,eq} - C_m(t=0)}. \tag{8}$$

Eq. (7) then leads to an exponential solution

$$C^*(t) = 1 - e^{-t/\tau} \quad \text{where } \tau = \frac{r^{3/2}}{3}\sqrt{\frac{2}{\kappa \nu}}. \tag{9}$$

Following our experimental results, we evaluate the degree of equilibration using three different values for the local speed of the drops and the speed at which the cloud of drops is entrained. The reference case corresponds to the standard iron rain scenario with a cloud of drops with a uniform radius $R_{cap}$, and where the local and global speeds are the corresponding Newtonian speed. Two other scenarios based on our experimental results are investigated. The local speed is given in one case by the Newtonian speed for each drop whose radius follows a Gamma distribution, and in the other case by the size-speed distribution results presented in Fig. 8, where we are assuming that the distribution does not depend on the large scale parameters such as the mean diameter and velocity of the drop cloud. In both cases, the global speed is the Newtonian velocity of the initial 10 km radius diapir. This estimate agrees with our present experimental results, as shown, for example, in Fig. 7. The global sedimentation speed, however, probably decreases over time because of the progressive entrainment of ambient fluid, as shown by Deguen et al. (2011, 2014). This effect is not seen here, possibly because of the limited size of our container. Corresponding equilibration results for the three models are shown in Fig. 9.

In all cases, the entire distribution of drops fully equilibrates before reaching the bottom of the magma ocean. However, the predicted depth of equilibration is 1 to 3 orders of magnitude larger when considering the scenarios derived from our fluid mechanics experiments compared to the idealized iron rain. This is the result of two combined effects highlighted by our laboratory experiments: droplet velocities are significantly larger than in the classical iron rain, and the drop size distribution puts a significant fraction of the metal phase in drops larger than $R_{cap}$, which implies a smaller surface of exchange between iron and silicate. As a result, equilibration will integrate a broader range of conditions regarding pressure and temperature, and the energy and mass exchanged by diffusion during the sinking of a particular metal droplet can occur substantively deeper within the magma ocean. Besides, for several elements, the partition coefficient depends on the pressure of equilibration. Expected changes in the depth of equilibration will also change their final repartition between core and mantle.

## 8. Conclusions and open questions

Our laboratory experiments on the fragmentation of gallium drops falling through glycerol shed new light on the dynamics of the iron sedimentation process that likely occurs during a terrestrial body's final accretionary stages. The classical iron rain scenario considers a population of spherical drops with a single characteristic radius that fall towards the bottom of the magma ocean at a unique velocity without any further change. In contrast, here we find that the fragmentation of an initially large diapir actually gives rise to a variety of stable shapes, a large distribution of sizes and velocities, and an intense internal dynamics within the cloud with the superimposition of further fragmentations and merging. Thus, we argue that previous models of chemical and thermal equilibration processes can only be accurate in a statistical mean sense (e.g. Rubie et al., 2003; Samuel et al., 2010). On the basis of our simple equilibration model, we still predict a complete equilibration before reaching the core, but at a significantly deeper depth. One should also keep in mind that the probability of a "strange" event, i.e. an anomalously large diapir or an anomalously slow falling velocity, is statistically possible, especially for large viscosity ratios.

Additional experiments are necessary to complement the conclusions drawn here, notably with a larger tank to avoid confinement effects and to allow for initially larger diapirs. Also it now appears necessary to take into account, in more evolved models of equilibration, the complex internal dynamics between drops inside the clouds, including the observed inverse cascade and the global sedimentation dynamics. It is also necessary, in addition to the first study for fixed-shape spherical drops by Ulvrová et al. (2011), to account for the very intense internal dynamics inside and outside large drops, which both stabilizes and deforms them, and should increase the equilibration process by advection.

All these effects clearly deserve further studies that are beyond the scope of this paper. Finally, our experiments have highlighted the importance of the viscosity ratio on the fluid dynamics of the fragmentation and sedimentation processes. As in Earth, the heat brought by the conversion of gravitational and kinetic energy during accretion is not negligible (see e.g. Tonks and Melosh, 1992; Samuel et al., 2010), it would now be interesting to study the strong coupling between the heating by viscous damping of the intense flows caused by the fall of iron diapirs, the changes in the ambient viscosity induced by this thermal evolution, and the corresponding evolution of the drop size distribution.

## Acknowledgements

We thank Professor E. Villermaux for helpful discussions. M.L.B. acknowledges financial support from the European Commission, Research Executive Agency, Marie Curie Actions (project FP7-PEOPLE-2011-IOF-298238). J.M. is funded by Agence Nationale de la Recherche (Accretis decision No. ANR-10-PDOC-001-01). J.M.A. and the UCLA SpinLab are supported by the NSF Geophysics Program.

## References

Abe, Y., Matsui, T., 1985. The formation of an impact-generated $H_2O$ atmosphere and its implications for the thermal history of the Earth. J. Geophys. Res. 90, 545–559.

Bonometti, T., Magnaudet, J., 2006. Transition from spherical cap to toroidal bubbles. Phys. Fluids 18, 052102.

Boyet, M., Carlson, R.W., 2005. $^{142}$Nd evidence for early (>4.53 Ga) global differentiation of the silicate Earth. Science 309, 576–581.

Boyet, M., Blichert-Toft, J., Rosing, M., Storey, M., Télouk, P., Albarède, F., 2003. $^{142}$Nd evidence for early Earth differentiation. Earth Planet. Sci. Lett. 214, 427–442.

Dahl, T.W., Stevenson, D.J., 2010. Turbulent mixing of metal and silicate during planet accretion and interpretation of the Hf–W chronometer. Earth Planet. Sci. Lett. 295, 177–186.

Deguen, R., Landeau, M., Olson, P., 2014. Turbulent metal–silicate mixing, fragmentation, and equilibration in magma oceans. Earth Planet. Sci. Lett. 391, 274–287. http://dx.doi.org/10.1016/j.epsl.2014.02.007.

Deguen, R., Olson, P., Cardin, P., 2011. Experiments on turbulent metal–silicate mixing in a magma ocean. Earth Planet. Sci. Lett. 310, 303–313.

Harper, C., Jacobsen, S., 1996. Evidence for $^{182}$Hf in the early solar system and constraints on the timescale of terrestrial accretion and core formation. Geochim. Cosmochim. Acta 60, 1131–1153.

Ichikawa, H., Labrosse, S., Kurita, K., 2010. Direct numerical simulation of an iron rain in the magma ocean. J. Geophys. Res. 115, B01404.

Karato, S.-I., Murthy, V., 1997. Core formation and chemical equilibrium in the Earth—I. Physical considerations. Phys. Earth Planet. Inter. 100, 61–79.

Kaula, W.M., 1979. Thermal evolution of Earth and moon growing by planetesimal impacts. J. Geophys. Res. 84, 999–1008.

King, E.M., Aurnou, J.M., 2013. Turbulent convection in liquid metal with and without rotation. Proc. Natl. Acad. Sci. USA 110 (17), 6688–6693.

Kleine, T., Mezger, K., Münker, C., Palme, H., Bischoff, A., 2004. $^{182}$Hf–$^{182}$W isotope systematics of chondrites, eucrites, and martian meteorites: chronology of core formation and early mantle differentiation in Vesta and Mars. Geochim. Cosmochim. Acta 68, 2935–2946.

Lee, D.-C., Halliday, A.N., 1996. Hf–W isotopic evidence for rapid accretion and differentiation in the early solar system. Science 274, 1876–1879.

Merk, R., Breuer, D., Spohn, T., 2002. Numerical modeling of $^{26}$Al-induced radioactive melting of asteroids considering accretion. Icarus 159, 183–191.

Monteux, J., Coltice, N., Dubuffet, F., Ricard, Y., 2007. Thermo-mechanical adjustment after impacts during planetary growth. Geophys. Res. Lett. 34, L24201.

Monteux, J., Ricard, Y., Coltice, F., Dubuffet, N., Ulvrová, M., 2009. A model of metal–silicate separation on growing planets. Earth Planet. Sci. Lett. 287, 353–362.

Morbidelli, A., Lunine, J., O'Brien, D., Raymond, S., Walsh, K., 2012. Building terrestrial planets. Annu. Rev. Earth Planet. Sci. 40, 251–275.

Neumann, W., Breuer, D., Spohn, T., 2012. Differentiation and core formation in accreting planetesimals. Astron. Astrophys. 543, A141.

Ohta, M., Yamaguchi, S., Yoshida, Y., Sussman, M., 2010. The sensitivity of drop motion due to the density and viscosity ratio. Phys. Fluids 22, 072102.

Reese, C., Solomatov, V., 2006. Fluid dynamics of local martian magma oceans. Icarus 184, 102–120.

Rubie, D.C., Melosh, H., Reid, J., Liebske, C., Righter, K., 2003. Mechanisms of metal–silicate equilibration in the terrestrial magma ocean. Earth Planet. Sci. Lett. 205, 239–255.

Rubie, D.C., Nimmo, F., Melosh, H.J., 2007. Formation of Earth's core. In: Treatise on Geophysics. Elsevier, pp. 51–90.

Safronov, V.S., 1978. The heating of the Earth during its formation. Icarus 33, 3–12.

Samuel, H., 2012. A re-evaluation of metal diapir breakup and equilibration in terrestrial magma oceans. Earth Planet. Sci. Lett. 313, 105–114.

Samuel, H., Tackley, P., Evonuk, M., 2010. Heat partitioning during core formation by negative diapirism in terrestrial planets. Earth Planet. Sci. Lett. 290, 13–19.

Solomatov, V.S., 2000. Fluid dynamics of a terrestrial magma ocean. In: Origin of the Earth and Moon. University of Arizona Press, pp. 323–338.

Stevenson, D.J., 1990. Fluid dynamics of core formation. In: Origin of the Earth. Oxford University Press, pp. 231–249.

Tonks, B., Melosh, J., 1992. Core formation by giant impacts. Icarus 100, 326–346.

Tonks, B., Melosh, J., 1993. Magma ocean formation due to giant impacts. J. Geophys. Res. 98, 5319–5333.

Ulvrová, M., Coltice, N., Ricard, Y., Labrosse, S., Dubuffet, F., Velimský, J., Srámek, O., 2011. Compositional and thermal equilibration of particles, drops, and diapirs in geophysical flows. Geochem. Geophys. Geosyst. 12, 1–11.

Villermaux, E., Bossa, B., 2009. Single-drop fragmentation determines size distribution of raindrops. Nat. Phys. 5, 697–702.

Walter, M., Tronnes, R., 2004. Early Earth differentiation. Earth Planet. Sci. Lett. 225, 253–269.

Yoshino, T., Walter, M., Katsura, T., 2003. Core formation in planetesimals triggered by permeable flow. Nature 422, 154–157.